RSC Advances

PAPER

View Article Online
View Journal | View Issue

Cite this: *RSC Adv.*, 2022, **12**, 15420

Research on the stability of luminescence of $CsPbBr_3$ and Mn:$CsPbBr_3$ PQDs in polar solution

Mou-Ce Jiang and Chun-Yang Pan *

Received 4th April 2022
Accepted 15th April 2022

DOI: 10.1039/d2ra02165j

rsc.li/rsc-advances

Mn:$CsPbBr_3$ PQDs are achieved by hot injection method. As the amount of Mn doping is gradually increased, the photoluminescence (PL) spectra shows a slight blue shift. Mn-doped PQDs exhibit higher quantum efficiency of 83.9% and longer lifetimes of 267 ns. The stability test was performed to assess the susceptibility of the PQDs to polar solutions. It was figured out that although the stabilities of $CsPbBr_3$ PQDs and Mn-doped PQDs decreased as the polarity of solution increased, Mn-doped PQDs still maintained higher PL intensity than undoped PQD. Notably, 73% PL intensity of Mn:PQDs was maintained which is nearly three times as much as undoped PQDs in water. We found polarity would induce drastic degradation of $CsPbBr_3$ QDs. The steady-state spectroscopy, transmission electron microscopy (TEM), and X-ray diffraction (XRD) verified that $CsPbBr_3$ QDs tend to aggregate to form larger particles under continuous light soaking. Our work reveals the main origin of instability in $CsPbBr_3$ QDs and provides reference to engineering such QDs towards optimal device application.

1. Introduction

The low cost, high photoluminescence quantum yields (PLQYs), and narrow and adjustable emission spectra of perovskite quantum dots (PQDs) make them attractive emitting materials for illumination and display applications.[1–4] In recent years, $CsPbX_3$ PQDs (X = Cl, Br, I) have attracted a great deal of attention from materials scientists as promising optoelectronic materials.[5–10] Compared to organic–inorganic hybrid perovskite materials, all-inorganic perovskites have the advantages of simple preparation and good stability.[11–16]

Despite plenty of advantages, the toxic nature of Pb and limited tolerance of all inorganic perovskites to moisture, ultraviolet (UV) light and the adjacent environment, cannot be ignored.[17–22] It is very urgent to figure out some approaches to solve these the worrying issues. $CsPbX_3$ can be doped with heterogeneous metal ions to replace Pb^{2+}, thus reducing the amount of Pb.[23–26] Researchers also figured out that the doped ions can bring about new electric, optical, and magnetic properties.[27–30] Kim *et al.* reported Ni^{2+}-doped $CsPbBr_3$ PQDs in 2021. The stability of the Ni:$CsPbBr_3$ PQDs with distinct Ni/Pb ratios against moisture and UV light was tested. Doping with Ni^{2+} improved the stability of PQDs. Further, the Ni:$CsPbBr_3$ PQDs exhibited compatibility with real-world applications under harsh conditions.[31] Zhou *et al.* successfully doped Zn^{2+} ions into $CsPbBr_3$ PQDs by ligand-assisted reprecipitation method, exhibiting an 85% enhancement of the PLQYs. In addition, the optimized energy level alignment *via* Zn doping facilitates the carrier balance in the devices, improving the efficiencies. The obtained $CsPbBr_3$:Zn-based PeLED reaches a high luminance of 3124 cd m^{-2} and a maximum external quantum efficiency of 0.85%, which are excellent among those of $CsPbBr_3$-based PeLED. The results demonstrate that Zn doping significantly enhances the performance of PeLED, which increases the potential of these inverted PeLEDs connected with n-type TFTs towards practical applications.[32] Among them, Mn^{2+} is an important choice, which can not only reduce Pb content to a certain extent but also reduce photon recycling, improve PLQYs, and expand luminous color gamut. An orange luminescence band due to the d–d transition of Mn^{2+} is introduced in addition to the intrinsic band-edge excitonic fluorescence. As well established previously, the efficient energy transfer from PQDs to Mn^{2+} only occurs when the Mn^{2+} content is high enough.[33,34] Mn^{2+} doping brings many benefits to PQDs, however, it's regrettable that the stability of Mn-doped $CsPbBr_3$ in polar solutions hasn't been studied in preceding researches, which is critical to its application in various conditions.

In this work, we successfully synthesized partially Mn-doped $CsPbBr_3$ by hot injection technique.[35–42] Then we demonstrate the Mn:$CsPbMnBr_3$ PQDs with a Mn substitution ratio up to 38%. The introduction of Mn^{2+} significantly increased the formation energy of Pb, Br, and Cs vacancies.[43,44] The PL lifespan was longer with Mn^{2+} doping, indicating the inhibition of non-radioactive recombination upon doping.[45] Besides the reduction of lead content, the as-prepared PQDs maintain the orthorhombic crystalline structure of the $CsPbBr_3$ host and exhibit strong PL emission of Pb-based PQDs.[46–49] Mn^{2+} doping enhances the PLQYs of $CsPbBr_3$ from 52.6% to 83.9%. Finally,

School of Light Industry and Chemical Engineering, Guangdong University of Technology, Guangzhou, Guangdong 510006, China. E-mail: panchuny@gdut.edu.cn; Tel: +86-020-39322231

three polar solvents of acetone, *N*,*N*-dimethylformamide (DMF), water, were selected to analyze the stabilities of $CsPbBr_3$ and Mn:$CsPbBr_3$. According to our experimental results, the Mn-doped $CsPbBr_3$ is superior to its undoped counterpart in terms of stability in polar solutions.

2. Results and discussion

2.1. Structure and composition of Mn-doped PQDs

Mn:$CsPbBr_3$ PQDs with different Mn^{2+} doping concentrations were prepared by the hot injection method reported previously. Five samples with Mn : Pb ratios are 0 : 1, 1 : 1, 2.5 : 1, 3.5 : 1 and 5 : 1, TEM images of the resulting Mn:$CsPbBr_3$ PQDs are shown in Fig. 1a–e, respectively. Five samples with Mn/Pb ratios of 0, 1.25, 2.5, 3.75, and 5 exhibited lattice constants of 5.78 Å, 5.73 Å, 5.65 Å, 5.59 Å, and 5.56 Å, respectively. All the prepared samples exhibited excellent crystallinity, as observed in the highresolution (HR-TEM) image, and the inter-planar distance of the (100) plane decreased from 5.77 Å to 5.56 Å depending on the feed of $MnBr_2$. The lattice shrinkage of the Mn^{2+} iondoped $CsPbBr_3$ PNCs is mainly due to the synergistic effect of replacing the larger Pb^{2+} ions (1.19 Å) with smaller Mn^{2+} ions (0.67 Å). The corresponding HRTEM images of the Mn:$CsPbBr_3$ PQDs are shown in Fig. 1a–e. Elemental mapping and energy dispersive X-ray spectroscopy (EDS) (Fig. 1f) were performed for a typical Mn : Pb ratio of 2.5 for Mn-doped $CsPbBr_3$ PQDs. To confirm the integration of guest Mn^{2+} cations, the chemical composition of Mn:$CsPbBr_3$ PQDs (Mn : Pb = 2.5) was analyzed by EDS. The elements Cs, Pb, Mn, and Br were identified in Mn:$CsPbBr_3$ PQDs. The four target elements were evenly distributed throughout the selection region, indicating successful synthesis of Mn:$CsPbBr_3$ PQDs and effective doping of Mn^{2+}.

Fig. 2a shows the XPS results, which depict the change in binding energy according to the doping element. The XPS spectrum reveals signals of the Cs, Pb, Br, and Mn elements in the Mn-doped $CsPbBr_3$ PQDs, and the corresponding high-resolution XPS spectrum shows a typical Mn 2P signal (Fig. 2b).

Selected area electron diffraction (SAED) patterns of the Mn:$CsPbBr_3$ also shows the presence of tetragonal (100) and (200) surfaces (Fig. 3a), confirming that the perovskite structure has not been destroyed. XRD patterns of the $CsPbBr_3$ doped with different concentrations of Mn^{2+} are shown in Fig. 3b. With increased Mn doping, there was no overall structural change.

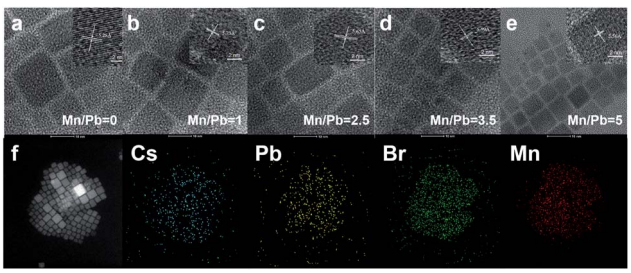

Fig. 1 (a) TEM images of $CsPbBr_3$ and (b)–(e) Mn:$CsPbBr_3$PQDs (Mn : Pb = 1 to 5). (f) Elemental mapping images of the Mn:$CsPbBr_3$ PQDs (Mn : Pb = 2.5).

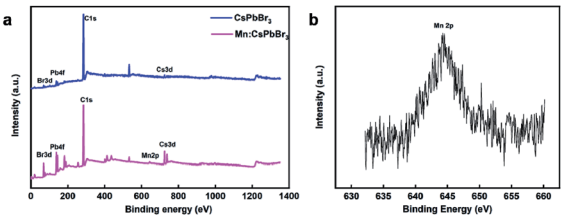

Fig. 2 (a) XPS of Mn:$CsPbBr_3$PQDs (Mn : Pb = 2.5). (b) High-resolution XPS spectra for Mn 2p of Mn:$CsPbBr_3$ PQDs.

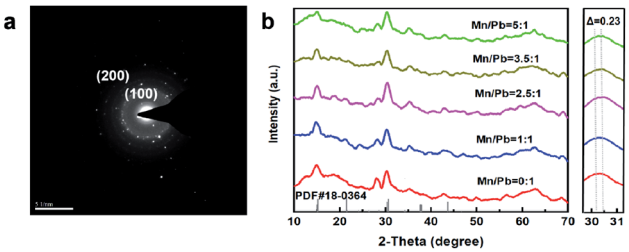

Fig. 3 (a) SAED pattern of Mn-doped $CsPbBr_3$ (Mn : Pb = 2.5). (b) XRD of Mn:$CsPbBr_3$PQDs (Mn : Pb from 0 to 5).

The orthorhombic $CsPbBr_3$ phase (PDF#18-0364, Fig. 3b) remained. The peak of (200) of the synthesized $CsPbBr_3$ PNCs shifted by 0.23° to the right when the Mn^{2+} concentration increased, indicating that the amount of Mn^{2+} dopant in the $CsPbBr_3$ PNCs increased. In addition, as the concentration of Mn increased, the intensity of the main peaks gradually increased. These results provide solid evidence for the efficient replacement of Mn^{2+} ions in the $CsPbBr_3$ PNC lattice. EDS were conducted to analyze the actual compositions of the Mn:$CsPbBr_3$ PQDs. When the feeding ratios are Mn : Pb = 1 : 1, Mn : Pb = 2.5 : 1, Mn : Pb = 3.5 : 1, and Mn : Pb = 5 : 1, the resulting products are $CsPb_{0.961}Mn_{0.039}Br_3$, $CsPb_{0.798}Mn_{0.202}Br_3$, $CsPb_{0.729}Mn_{0.271}Br_3$, and $CsPb_{0.616}Mn_{0.384}Br_3$, respectively (Table 1).

2.2 Optical properties

Fig. 4 shows the absorbance graph according to the Mn doping concentration. The absorption measurement results demonstrated that light of wavelength 500–513 nm was absorbed by the PQDs. Due to the decreased size of Mn:$CsPbBr_3$ PQDs, their UV-vis absorption spectra show a gradual blue shift with the increase Mn-to-Pb molar feed ratio. Since no new absorption band was observed after Mn doping, it is presumed that Mn doping has a negligible effect on the electronic structure of $CsPbBr_3$ PQDs.

Table 1 EDS of Mn:$CsPbBr_3$PQDs (Mn : Pb from 1 to 5)

Mn : Pb	1 : 1	2.5 : 1	3.5 : 1	5 : 1
Mn	0.039	0.202	0.271	0.384
Pb	0.961	0.798	0.729	0.616

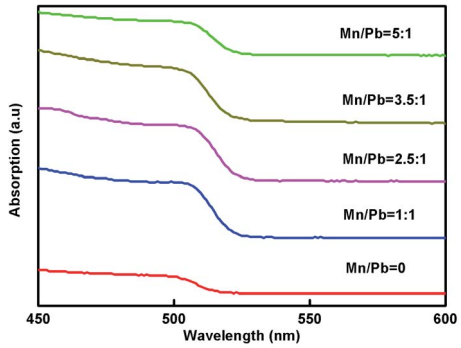

Fig. 4 Absorption of $CsPbBr_3$ and Mn:$CsPbBr_3$ PQDs.

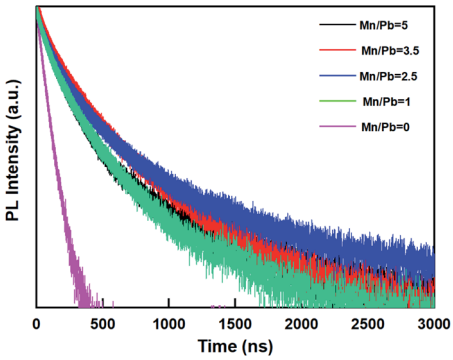

Fig. 6 Time-resolved PL decays of fresh $CsPbBr_3$ and Mn:$CsPbBr_3$ PQDs.

Fig. 5a manifests the PL measurements. 508–518 nm marked the wavelength band of emitted light. The average half width proved to be 20.4 nm, which revealed high color purity. With the increasing doping concentration, because of the quantum confinement effect, the emission wavelength was going through a blue shift from 518 to 508 nm. A change in the energy level resulting from doping concentration resulted in a reduction in emission wavelength at the rate of 3–10 nm compared with the undoped sample. The PL intensity was on a gradual increase when substituted concentration of Mn^{2+} ions was growing larger. Nonetheless, the others PL peaks (Mn : Pb = 3.5, 5) was decreasing. Particularly speaking, the PL peak intensity of the sample (Mn : Pb = 2.5), when compared with the intensity of the undoped sample, was increasing at the rate of 3.8 times. According to Fig. 5b, the gradual conversion color converted from green to blue; the most striking luminous intensity was shown with the Mn : Pb = 2.5. The highest quantum efficiency could be seen at an Mn : Pb of 2.5. The sample specialized the quantum efficiency was expressed at a doping ratio of 2.5 (Mn : Pb = 2.5, ≈83.9%), which differed by ≈27% with no doping (Mn : Pb = 0, ≈56.7%). For Mn : Pb = 3.5, however, the quantum efficiency decreased dramatically, indicating that the Mn^{2+} ion has a very strong effect upon the optical properties of PQDs. From the differences in defect levels offered by the doping material, a proper doping concentration able to gain high quantum efficiency can be attained. These results show that Mn^{2+} doping forms a Mn–Br ion pair to fill the Pb–Br ion vacancy, which effectively eliminates the non radiative recombination of excitons and improves the luminescence intensity of $CsPbBr_3$ quantum dots. As the Mn doping increasing, Mn–Mn ion pair appears. This phenomenon is observed in Pan's work of Ni^{2+} ion-doped $CsPbCl_xBr_{3-x}$ PQDs.[51]

The average lifetime for excitonic luminescence of $CsPbBr_3$ PQDs added Mn^{2+} ions is observed to increase from 43.2 ns to 267.6 ns compared to undoped $CsPbBr_3$ PQDs. The radiative and non-radiative decay rates can also be calculated using PLQY and the average life. The radiative rate decreased slightly from 0.0662 ns^{-1} to 0.0372 ns^{-1}, and the non radiative recombination, which must be controlled for optical properties, significantly decreased from 0.0506 to 0.0077 ns^{-1}. Therefore, the improvement in fluorescence performance can be attributed to the greatly reduced non-radiative attenuation of the incorporation of Mn:$CsPbBr_3$ PQDs.

For acetone, the PL intensity of the initial reference sample after 2 h was 20% lower than the initial value (Fig. 7a). In contrast, the steady-state PL intensity at 2 h was 11.0%, lower than the initial value of Mn:$CsPbBr_3$ PQDs (Fig. 6b). The decrease in the steady-state PL intensity of $CsPbBr_3$ is more noticeably than that of Mn:$CsPbBr_3$ PQDs in acetone, which indicates that Mn doping enhanced the stability of $CsPbBr_3$ PQDs.

Fig. 8 shows stability of pristine $CsPbBr_3$ and Mn:$CsPbBr_3$ PQDs (Mn : Pb = 2.5) in DMF. The PL intensity of $CsPbBr_3$ PQDs lower than 50% in DMF after 2 h. While PL intensity of Mn:$CsPbBr_3$ PQDs maintain 76%. As the polarity improved, the enhancement of stability of Mn^{2+} doping is more pronounced.

To investigate the water stability of the pre-synthesized Mn:$CsPbBr_3$ PQDs, the PQD solution was injected with a 5% volume ratio of deionized water (DIW). For comparison, the

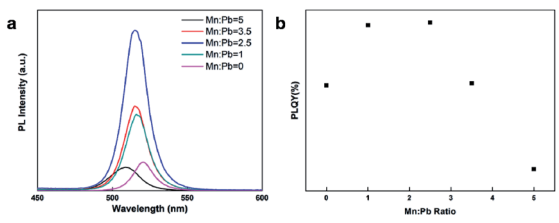

Fig. 5 (a) PL peaks of pristine and Mn:$CsPbBr_3$ PQDs with different Mn : Pb ratios; the insets show the corresponding normalized PL spectra. (b) PLQY with various Mn : Pb feed molar ratios of 0, 1, 2.5, 3.5, 5; the insets show the photograph of the Mn:$CsPbBr_3$ PQDs in hexane solution under an irradiation of a 360 nm UV lamp.

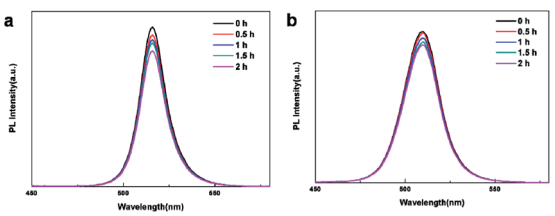

Fig. 7 (a) PL spectra of the pristine $CsPbBr_3$ and (b) Mn:$CsPbBr_3$ PQDs (Mn : Pb = 2.5) recorded at different time intervals in acetone.

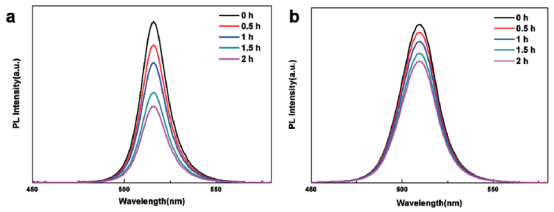

Fig. 8 (a) PL spectra of the pristine $CsPbBr_3$ and (b) Mn:$CsPbBr_3$ PQDs (Mn : Pb = 2.5) recorded at different time intervals in DMF.

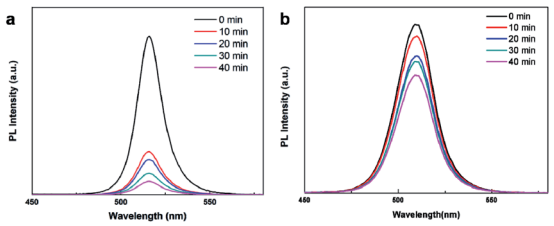

Fig. 9 (a) PL spectra of the pristine $CsPbBr_3$ and (b) Mn^{2+}-substituted $CsPbBr_3$ PQDs (Mn : Pb = 2.5) recorded at different time intervals in water.

measurements were performed for pristine $CsPbBr_3$ PQDs at the same concentration as the Mn:$CsPbBr_3$ PQD solution over time. A quantitative study was conducted by recording the PL evolution; the results are summarized in Fig. 9. The corresponding PL spectra of undoped $CsPbBr_3$ PQDs and Mn:$CsPbBr_3$ PQDs were documented at separate time intervals after the addition of DIW. For Mn:$CsPbBr_3$ PQDs (Mn : Pb = 2.5), fluorescence quenching was comparatively slow and retained more than 73% of its initial performance, even over longer test periods. The PL spectra of the $CsPbBr_3$ PQDs (Fig. 9a) and Mn:$CsPbBr_3$ PQDs (Fig. 9b) based on the moisture test are shown. As shown in Fig. 9a, a small weakening of the emission intensity for Mn:$CsPbBr_3$ PQDs was confirmed, but strong fluorescence was still observed. However, the $CsPbBr_3$ PQDs lost majority of their brightness in just 1 min of testing, gradually changing fluorescent from green to colorless. The efficiency of $CsPbBr_3$ PQDs decreased owing to the aggregation and decomposition of $CsPbBr_3$ PQDs, and the optical properties of $CsPbBr_3$ PQDs weakened as the half-width broadened. Based on the above results, we speculate that Mn^{2+} ions occupy the lead site, which makes the structure of PQDs more stable in polar solutions.

3. Experimental section

3.1 Materials

All chemicals were used as received without further purification. Cesium carbonate (Cs_2CO_3, 99.9%, Sigma-Aldrich), oleic acid (OA, 90%, Sigma-Aldrich), 1-octadecene (ODE, 90%, Sigma-Aldrich), $PbBr_2$ (99.9%, Maclin), $MnBr_2$ (99.9%, Maclin), and oleylamine (OAm, 70%, Sigma-Aldrich).

3.2 Synthesis of Cs-oleate

Cs_2CO_3 (0.05 g), OA (0.5 mL), and ODE (10 mL) were placed in a 100 mL three-necked round-bottom flask. Next, the mixture was heated at 110 °C for 1 h under vacuum to completely remove moisture and oxygen. After that, the reaction temperature was maintained at 120 °C under N_2 atmosphere and stirred until all Cs_2CO_3 reacted with OA to form Cs-oleate. A clear solution was obtained. Notably, Cs-oleate precipitated in the ODE at ambient temperature and had to be preheated to 100 °C before it could be used for the subsequent synthesis of PQDs.

3.3 Synthesis of $CsPbX_3$PQDs

The synthesis method of $CsPbX_3$ PQDs is similar to the approach of Protesescu *et al.*,[50] with a few insignificant modifications. In brief, 10 mL ODE and 0.2 mmol $PbBr_2$ were added to a 250 mL three-neck round-bottom flask and dried under vacuum at 110 °C for 1 h. The flask was purged with N_2, and OA (0.5 mL) and OAm (0.5 mL) preheated to 70 °C was injected into the flask. The flask was heated at 120 °C until PbX_2 completely reacted with OA and OAm. The temperature was then increased to 150 °C. The Cs-oleate precursor (0.8 mL) was quickly injected into the Pb-oleate. The solution was maintained at 150 °C for several seconds to allow the growth of the PQDs. The solution was cooled by soaking the flask in a cold-water bath.

3.4 Synthesis of Mn:$CsPbX_3$PQDs

The synthesis of the Mn-doped $CsPbX_3$ PQDs was performed in a manner similar to that of the $CsPbX_3$ PQDs, as described above. ODE (5 mL) and $PbBr_2$ were added to a 250 mL three-necked round-bottom flask and dried under vacuum at 110 °C for 1 h. All other steps remained the same.

3.5 Purification

The as-prepared $CsPbX_3$PQD and Mn-doped $CsPbX_3$PQD crude solutions were precipitated by centrifuging at 6000 rpm for 5 min. The colored supernatant was carefully discarded, and the precipitate was mixed with hexane (1.5 mL) using a vortex. The solution was centrifuged at 6000 rpm for 5 min. Finally, the PQDs were dispersed in hexane (1 mL) and centrifuged at 10 000 rpm for 2 min to remove any excess Cs-oleate, larger PQDs, and agglomerates. The precipitate was then collected and redispersed in hexane, resulting in a colloidal dispersion of the $CsPbX_3$ PQDs.

3.6 Characterization

The size, morphology, and crystallinity of the nanoparticles were characterized by field-emission transmission electron microscopy (FE-TEM, JEOL, JEM-F200) in EDS. TEM images were obtained using high-resolution transmission electron microscopy (HR-TEM, FEI, Tecnai 20). The lattice constant was determined from the HR-TEM images using GATAN software. The absorption spectra were obtained using a UV-vis spectrophotometer (Varian, Cary 50). PL excitation and emission spectra were measured using a steady-state spectrofluorometer (PTI, QuantaMaster) with an excitation wavelength of 360 nm. XRD patterns were collected on a powder diffractometer (Bruker New D8-Advance) with monochromatized Cu Kα radiation (λ = 1.5418 Å). XPS was performed using a ULVAC-PHI X-TOOL

instrument. PLQY was measured using a spectrofluorometer (JASCO, FP-8500) with an integrating sphere. Time-resolved PL experiments were performed using the TCSPC method. The samples in the solutions were excited using a 360 nm pulse (LDH-P-C-520, Picoquant). The time-resolved PL signals emitted from the samples were resolved using a monochromator and detected by a photomultiplier tube (PMT).

4. Conclusions

In this work, a hot-injection method help achieving $CsPbBr_3$ perovskite QDs which possessing a high Mn-doping ratio. Consequently the properties of Pb-based perovskite QDs were improved. In order to gain their enhanced stability, different Mn : Pb ratio of $CsPbBr_3$ PQDs structure was achieved. The Mn substitution ratio reaches 38%, which leads to an increase of 3.8 times of the steady-state PL intensity, the lifetime increase to 267 ns. In comparison to the undoped sample, the quantum efficiency achieved the improved as large of 30.6%. The stability of the Mn:$CsPbBr_3$ PQDs with distinct Mn : Pb ratios against polar solutions was tested. Doping with Mn^{2+} improved the stability of PQDs according to our research.

Conflicts of interest

The authors state that they have no conflicts of interest to declare.

Acknowledgements

This work was supported by the National Natural Science Foundation of China (No. 21671044).

Notes and references

1 X. Li, D. Yu, F. Cao, Y. Gu, Y. Wei, Y. Wu, J. Song and H. Zeng, Healing All-Inorganic Perovskite Films via Recyclable Dissolution–Recrystallization for Compact and Smooth Carrier Channels of Optoelectronic Devices with High Stability, *Adv. Funct. Mater.*, 2016, **26**, 5903–5912.

2 A. J. Nozik, Making the most of photons, *Nanophotonics*, 2009, **4**, 548–549.

3 J. Pan, L. N. Quan, Y. B. Zhao, W. Peng, B. Murali, S. P. Sarmah, M. J. Yuan, L. Sinatra, N. M. Alyami, J. K. Liu, E. Yassitepe, Z. Y. Yang, O. Voznyy, R. Comin, M. N. Hedhili, O. F. Mohammed, Z. H. Lu, D. H. Kim, E. H. Sargent and O. M. Bakr, Highly Efficient Perovskite-Quantum-Dot Light-Emitting Diodes by Surface Engineering, *Adv. Mater.*, 2016, **28**, 8718–8725.

4 Z. K. Tan, R. S. Moghaddam, M. L. Lai, P. Docampo, R. Higler, F. Deschler, M. Price, A. Sadhanala, L. M. Pazos, D. Credgington, F. Hanusch, T. Bein, H. J. Snaith and R. H. Friend, Bright light-emitting diodes based on organometal halide perovskite, *Nat. Nanotechnol.*, 2014, **9**, 687–692.

5 Q. A. Akkerman, V. D'Innocenzo, S. Accornero, A. Scarpellini, A. Petrozza, M. Prato and L. Manna, Tuning the Optical Properties of Cesium Lead Halide Perovskite Nanocrystals by Anion Exchange Reactions, *J. Am. Chem. Soc.*, 2015, **137**, 10276–10281.

6 W. C. He, Q. Q. Zhang, Y. F. Qi, J. Moore, P. Ray, N. Pradhan, X. C. Zhu, F. X. Han, T. Shahbazyan and Q. L. Dai, Synthesis and optical properties of doped $CsPbCl_3$ nanocrystals, *J. Nanopart. Res.*, 2021, **23**, 219.

7 G. Nedelcu, L. Protesescu, S. Yakunin, M. I. Bodnarchuk, M. J. Grotevent and M. V. Kovalenko, Fast Anion-Exchange in Highly Luminescent Nanocrystals of Cesium Lead Halide Perovskites ($CsPbX_3$, X = Cl, Br, I), *Nano Lett.*, 2015, **15**, 5635–5640.

8 X. L. Zhang, B. Xu, J. B. Zhang, Y. Gao, Y. J. Zheng, K. Wang and X. W. Sun, All-Inorganic Perovskite Nanocrystals for High-Efficiency Light Emitting Diodes: Dual-Phase $CsPbBr_3$-$CsPb_2Br_5$ Composites, *Adv. Funct. Mater.*, 2016, **26**, 4595–4600.

9 Y. Z. Zheng, X. Yuan, J. Yang, Q. Y. Li, X. X. Yang, Y. Fan, H. B. Li, H. L. Liu and J. L. Zhao, Cu doping-enhanced emission efficiency of Mn^{2+} in cesium lead halide perovskite nanocrystals for efficient white light-emitting diodes, *J. Lumin.*, 2020, **227**, 117586.

10 S. H. Zhou, C. W. Zhou, J. Y. Zhu, H. Huang, F. Hu, Q. L. Ye, J. Q. Zhong, X. X. Yang and H. Y. Mao, Enhanced field emission properties of $CsPbBr_3$ films by thermal annealing and surface functionalization with boron nitride, *Appl. Surf. Sci.*, 2022, **578**, 152116.

11 R. Yuan, Y. Cheng, S. Liu, L. Ding, H. Zhang, W. Xiang and X. Liang, Multicolour light-emitting diodes based on $CsPbX_3$ (X = Br, I) quantum dots glasses solid materials, *Mater. Lett.*, 2018, **229**, 290–292.

12 R. Han, Q. Zhao, J. Su, X. Zhou, X. Ye, X. Liang, J. Li, H. Cai, J. Ni and J. Zhang, Role of Methyl Acetate in Highly Reproducible Efficient $CsPbI_3$ Perovskite Quantum Dot Solar Cells, *J. Phys. Chem. C*, 2021, **125**, 8469–8478.

13 G. Nedelcu, L. Protesescu, S. Yakunin, M. I. Bodnarchuk, M. J. Grotevent and M. V. Kovalenko, Fast Anion-Exchange in Highly Luminescent Nanocrystals of Cesium Lead Halide Perovskites ($CsPbX_3$, X = Cl, Br, I), *Nano Lett.*, 2015, **15**, 5635–5640.

14 F. Yang, C. Wang, Y. Pan, X. Zhou, X. Kong and W. Ji, Surface stabilized cubic phase of $CsPbI_3$ and $CsPbBr_3$ at room temperature, *Chin. Phys. B*, 2019, **28**, 056402.

15 J. Chen, D. Liu, M. J. Al-Marri, L. Nuuttila, H. Lehtivuori and K. Zheng, Photo-stability of $CsPbBr_3$ perovskite quantum dots for optoelectronic application, *Sci. China Mater.*, 2016, **59**, 719–727.

16 H. W. Liu, Z. N. Wu, J. R. Shao, D. Yao, H. Gao, Y. Liu, W. L. Yu, H. Zhang and B. Yang, $CsPb_xMn_{1-x}Cl_3$ Perovskite Quantum Dots with High Mn Substitution Ratio, *ACS Nano*, 2017, **11**, 2239–2247.

17 W. Yan, J. Shen, Y. Zhu, Y. Gong, J. Zhu, Z. Wen and C. Li, $CsPbBr_3$ quantum dots photodetectors boosting carrier transport via molecular engineering strategy, *Nano Res.*, 2021, **14**, 4038–4045.

18 F. H. Ye, H. J. Zhang, W. Li, Y. Yan, J. L. Cai, R. S. Gurney, A. J. Pearson, D. Liu and T. Wang, Ligand-Exchange of

Low-Temperature Synthesized CsPbBr3 Perovskite toward High-Efficiency Light-Emitting Diodes, *Small Methods*, 2019, **3**, 3120–3126.

19 Y. Ahmed, B. Khan, M. Bilal Faheem, K. Huang, Y. Gao and J. Yang, Organic additives in all-inorganic perovskite solar cells and modules: from moisture endurance to enhanced efficiency and operational stability, *J. Energy Chem.*, 2022, **67**, 361–390.

20 J. K. Nam, S. U. Chai, W. Cha, Y. J. Choi, W. Kim, M. S. Jung, J. Kwon, D. Kim and J. H. Park, Potassium Incorporation for Enhanced Performance and Stability of Fully Inorganic Cesium Lead Halide Perovskite Solar Cells, *Nano Lett.*, 2017, **17**, 2028–2033.

21 Y. Gao, C. Luo, C. Yan, W. Li, C. A. Q. Liu and W. Q. Yang, Copper-doping defect-lowered perovskite nanosheets for deep-blue light-emitting diodes, *J. Colloid Interface Sci.*, 2022, **607**, 1796–1804.

22 F. Montanarella, K. M. McCall, K. Sakhatskyi, S. Yakunin, P. Trtik, C. Bernasconi, I. Cherniukh, D. Mannes, M. I. Bodnarchuk, M. Strobl, B. Walfort and M. V. Kovalenko, Highly Concentrated, Zwitterionic Ligand-Capped Mn^{2+}:$CsPb(Br_xCl_{1-x})_3$ Nanocrystals as Bright Scintillators for Fast Neutron Imaging, *ACS Energy Lett.*, 2021, **6**, 4365–4373.

23 F. Sui, M. Y. Pan, Z. Y. Wang, M. Chen, W. J. Li, Y. Shao, W. M. Li and C. L. Yang, Quantum yield enhancement of Mn-doped CsPbCl3 perovskite nanocrystals as luminescent down-shifting layer for CIGS solar cells, *Sol. Energy*, 2020, **206**, 473–478.

24 F. unlu, M. Deo, S. Mathur, T. Kirchartz and A. Kulkarni, Bismuth-based halide perovskite and perovskite-inspired light absorbing materials for photovoltaics, *J. Phys. D: Appl. Phys.*, 2022, **55**, 13002.

25 X. W. Zhou, Y. Zhao, W. Z. Huang, Y. Y. Wu, Z. E. Wu and G. F. He, Enhanced performance of inverted $CsPbBr_3$ nanocrystal LEDs via Zn (II) doping, *Org. Electron.*, 2021, **96**, 106253.

26 J. F. Cao, Z. D. Yin, Q. Pang, Y. X. Lu, X. Q. Nong and J. Z. Zhang, Modulating optical properties and interfacial electron transfer of CsPbBr3 perovskite nanocrystals via indium ion and chlorine ion co-doping, *J. Chem. Phys.*, 2021, **155**, 234701.

27 Y. J. Guo, J. Su, L. Wang, Z. H. Lin, Y. Hao and J. J. Chang, Improved Doping and Optoelectronic Properties of Zn-Doped $CsPbBr_3$ Perovskite through Mn Codoping Approach, *J. Phys. Chem. Lett.*, 2021, **12**, 3393–3400.

28 S. N. Liu, G. Z. Shao, L. Ding, J. M. Liu, W. D. Xiang and X. J. Liang, Sn-doped $CsPbBr_3$ QDs glasses with excellent stability and optical properties for WLED, *Chem. Eng. J.*, 2019, **361**, 937–944.

29 K. W. Ma, Y. H. Sheng, G. Z. Wang, X. W. Zhang, Y. S. Di, C. H. Liu, L. Y. Yu, L. F. Dong and Z. X. Gan, Stable and multicolor solid-state luminescence of Mn doped CsPb(Cl/Br)3 perovskite quantum dots and its application in light-emitting diodes, *J. Lumin.*, 2022, **243**, 118622.

30 Y. X. Zhu, B. B. Yang, Q. Lu, Y. Li, M. M. Shi and J. Zou, A Cyan Emitting $CsPbBr_3$ Perovskite Quantum Dot Glass with Bi Doping, *ECS J. Solid State Sci. Technol.*, 2020, **9**, 126003.

31 H. Kim, S. R. Bae, T. H. Lee, H. Lee, H. Kang, S. Park, H. W. Jang and S. Y. Kim, Enhanced Optical Properties and Stability of CsPbBr3 Nanocrystals Through Nickel Doping, *Adv. Funct. Mater.*, 2021, **31**, 2102770.

32 X. W. Zhou, Y. Zhao, W. Z. Huang, Y. Y. Wu, Z. E. Wu and G. F. He, Enhanced performance of inverted $CsPbBr_3$ nanocrystal LEDs via Zn (II) doping, *Org. Electron.*, 2021, **96**, 106253.

33 Y. Ouyang, X. X. Jiang, F. Jiang, L. H. Li, H. P. Zhao, C. Zhang, M. Zheng, W. H. Zheng, Y. Jiang, X. L. Zhu, Y. X. Feng and X. J. Zhuang, Light-Soaking Induced Optical Tuning in Rare Earth-Doped All-Inorganic Perovskite, *Adv. Funct. Mater.*, 2021, 2107086.

34 M. J. Patel, D. Raval, S. K. Gupta and P. N. Gajjar, First-Principles Study of Mn-Doped and Nb-Doped $CsPbCl_3$ Monolayers as an Absorber Layer in Solar Cells, *J. Phys. Chem. Lett.*, 2021, **12**, 7319–7327.

35 M. Zeng, F. Locardi, D. Mara, Z. Hens, R. Van Deun and F. Artizzu, Switching on near-infrared light in lanthanide-doped $CsPbCl_3$ perovskite nanocrystals, *Nanoscale*, 2021, **13**, 8118–8125.

36 Y. Zheng, X. Yuan, J. Yang, Q. Li, X. Yang, Y. Fan, H. Li, H. Liu and J. Zhao, Cu doping-enhanced emission efficiency of Mn^{2+} in cesium lead halide perovskite nanocrystals for efficient white light-emitting diodes, *J. Lumin.*, 2020, **227**, 117586.

37 D. Q. Chen, S. Zhou, F. F. Tian, H. T. Ke, N. Z. Jiang, S. J. Wang, Y. Z. Peng and Y. Liu, Halogen-Hot-Injection Synthesis of Mn-Doped $CsPb(Cl/Br)_3$ Nanocrystals with Blue/Orange Dual-Color Luminescence and High Photoluminescence Quantum Yield, *Adv. Opt. Mater.*, 2019, **7**, 1901082.

38 A. Forde, S. A. Thomas, R. J. Petersen, S. L. Brown, D. S. Kilin and E. K. Hobbie, Size-Dependent Doping Synergy and Dual-Color Emission in $CsPb_{1-x}Mn_xCl_3$ Nanocrystals, *J. Phys. Chem. C*, 2021, **125**, 18849–18856.

39 J. Ghosh, M. Hossain and P. K. Giri, Origin and tunability of dual color emission in highly stable Mn doped $CsPbCl_3$ nanocrystals grown by a solid-state process, *J. Colloid Interface Sci.*, 2020, **564**, 357–370.

40 S. K. Mehetor, H. Ghosh, B. Hudait, N. S. Karan, A. Paul, S. Baitalik and N. Pradhan, Reversible Color Switching in Dual-Emitting Mn(II)-Doped CsPbBr3 Perovskite Nanorods: Dilution versus Evaporation, *ACS Energy Lett.*, 2019, **4**, 2353–2359.

41 W. Z. Wang, J. K. Li, G. B. Duan, H. Zhou, Y. Z. Lu, T. Yan, B. Q. Cao and Z. M. Liu, Study on the Mn-doped CsPbCl3 perovskite nanocrystals with controllable dual-color emission via energy transfer, *J. Alloys Compd.*, 2020, **821**, 153568.

42 L. Bao, W. Liu, Y. Chen, Y. Zhang and Y. Zhang, Enhanced blue emission from CsPb(Br/Cl)3 perovskite nanocrystals by localized surface plasmon resonance of Au nanoparticles, *J. Mater. Chem. C*, 2021, **9**, 5182–5189.

43 L. M. Dong, Z. Chen, L. Ye, Y. Yu, J. B. Zhang, H. Liu and J. F. Zang, Gram-scale synthesis of all-inorganic perovskite quantum dots with high Mn substitution ratio and enhanced dual-color emission, *Nano Res.*, 2019, **12**, 1733–1738.

44 M. F. Abdelbar, M. El-Kemary and N. Fukata, Downshifting of highly energetic photons and energy transfer by Mn-doped perovskite CsPbCl3 nanocrystals in hybrid organic/silicon nanostructured solar cells, *Nano Energy*, 2020, **77**, 105163.

45 W. He, Q. Zhang, Y. Qi, J. Xiong, P. Ray, N. R. Pradhan, T. V. Shahbazyan, F. Han and Q. Dai, Luminescence properties of CsPbBr3:Mn nanocrystals, *J. Nanopart. Res.*, 2021, **23**, 332–337.

46 Z. Tan, J. Pang, G. Niu, J.-H. Yuan, K.-H. Xue, X. Miao, W. Tao, H. Zhu, Z. Li, H. Zhao, X. Du and J. Tang, Tailoring the electron and hole dimensionality to achieve efficient and stable metal halide perovskite scintillators, *Nanophotonics*, 2021, **10**, 2249–2256.

47 Y. Lou, Y. Niu, D. Yang, Q. Xu, Y. Hu, Y. Shen, J. Ming, J. Chen, L. Zhang and Y. Zhao, Rod-shaped thiocyanate-induced abnormal band gap broadening in SCN−doped $CsPbBr_3$ perovskite nanocrystals, *Nano Res.*, 2018, **11**, 2715–2723.

48 D. Parobek, B. J. Roman, Y. Dong, H. Jin, E. Lee, M. Sheldon and D. H. Son, Exciton-to-Dopant Energy Transfer in Mn-Doped Cesium Lead Halide Perovskite Nanocrystals, *Nano Lett.*, 2016, **16**, 7376–7380.

49 S. Ye, M. Yu, M. Zhao, J. Song and J. Qu, Low temperature synthesis of high-quality all-inorganic cesium lead halide perovskite nanocrystals in open air and their upconversion luminescence, *J. Alloys Compd.*, 2018, **730**, 62–70.

50 L. Protesescu, S. Yakunin, M. I. Bodnarchuk, F. Krieg, R. Caputo, C. H. Hendon, R. X. Yang, A. Walsh and M. V. Kovalenko, Nanocrystals of Cesium Lead Halide Perovskites ($CsPbX_3$, X = Cl, Br, and I): Novel Optoelectronic Materials Showing Bright Emission with Wide Color Gamut, *Nano Lett.*, 2015, **15**, 3692–3696.

51 G. Pan, X. Bai, W. Xu, X. Chen, Y. Zhai, J. Zhu, H. Shao, N. Ding, L. Xu, B. Dong, Y. Mao and H. Song, Bright Blue Light Emission of Ni^{2+} Ion-Doped $CsPbCl_xBr_{3-x}$ Perovskite Quantum Dots Enabling Efficient Light-Emitting Devices, *ACS Appl. Mater. Interfaces*, 2020, **12**, 14195–14202.